TUDelft

Delft University of Technology

On the use of full particle trajectories and vorticity transport for dense velocity field reconstruction

Schneiders, Jan; Scarano, Fulvio

Publication date
2018
Document Version
Final published version
Published in
Proceedings of the 19th international symposium on application of laser and imaging techniques to fluid mechanics

Citation (APA)
Schneiders, J., & Scarano, F. (2018). On the use of full particle trajectories and vorticity transport for dense velocity field reconstruction. In *Proceedings of the 19th international symposium on application of laser and imaging techniques to fluid mechanics*

Important note
To cite this publication, please use the final published version (if applicable).
Please check the document version above.

On the use of full particle trajectories and vorticity transport for dense velocity field reconstruction

Jan F.G. Schneiders[1], Fulvio Scarano[1,*]

1: Dept. of Aerospace Engineering, TU Delft, The Netherlands

* Correspondent author: f.scarano@tudelft.nl

Keywords: Large-scale PIV, HFSB, on-site, sports aerodynamics

ABSTRACT

A procedure is proposed to reconstruct the instantaneous velocity field from full particle trajectories in a data assimilation framework that includes the vorticity transport equation. The technique is christened as *time-segment assimilation* (TSA). The work addresses the common problem of low seeding concentration in 3D experiments, usually leading to limited spatial resolution. In the present study the measurement fidelity and spatial resolution are increased by considering finite time-segments as a whole for instantaneous velocity reconstruction.

The use of a time-segment for velocity field reconstruction from measurement data extends previously proposed data assimilation techniques that consider only instantaneous measurement data (e.g. VIC+ and FlowFit), to use finite measurement time-segments. The assessment with sinusoids indicates lower errors due to modulation. However, the appearance of a range of amplified peaks is not fully understood. In the case of a simulated turbulent boundary layer measurement more vortical structures are recovered when a longer time-segment is used for the velocity field reconstruction.

1. Introduction

In comparison to tomographic PIV, volumetric particle tracking has been shown the potential to achieve a higher spatial resolution, first by avoiding the spatial filtering introduced by cross-correlation and secondly because of the use of dense interpolations using governing equations. Examples of the latter interpolation techniques are divergence free fitting (de Silva et al. 2013; Schiavazzi et al. 2014; amongst others), vorticity equation based fitting (VIC+, Schneiders et al. 2015) and FlowFit (Gesemann et al. 2016). The latter examples employ the momentum equation in addition to the continuity equation. In case of divergence free interpolation, only instantaneous velocity measurement data is used for the interpolation. The VIC+ and FlowFit techniques, instead make use of the additional information provided by the instantaneous velocity material derivative obtained from particle tracking techniques. As a result, the ensemble of data used for velocity interpolation to a grid is doubled. This allows in turn for velocity estimation at scales below the average distance among neighboring particles. Recent works (Schneiders and Scarano 2016; Schneiders et al. 2017) have shown the ability of the VIC+ analysis to resolve the process of turbulent dissipation, otherwise systematically underestimated when using cross-correlation analysis from tomographic PIV.

Although reconstructing the velocity field with an increased data ensemble from

instantaneous measurements (i.e. velocity and material derivative) is already considered as an advantage, one can argue that the measured data is not exploited to its full potential. The main question is whether knowledge of the velocity along a finite time segment (as a result of tracers trajectories measurement) can possibly yield a further improvement of the velocity field estimation, primarily in terms of spatial resolution and temporal consistency. This concept should not be confused with the fact that the information used to obtain accurate tracers velocity estimation already takes into account a finite trajectory. The most accepted approach is to use polynomials to fit the particle discrete positions recorded along their trajectory, which increases the measurement dynamic range (Novara and Scarano, 2013, among others).

The concept of flow reconstruction on a dense grid making use of particle tracking measurements over an extended number of snapshots was preliminarily investigated in the simplified condition of two-dimensional flow motions (Schneiders et al. 2016). The results suggested that the use of a finite time-segment increases fidelity of the instantaneous velocity fields, beyond what would be possible using velocity and its material derivative at a given time instant.

In the present work, a formulation of the approach for use in unsteady three-dimensional flows is introduced. The procedure is referred to as *time-segment assimilation* (TSA), because it reconstructs the velocity field in a data assimilation framework, by making use of a time-segment of velocity measurement data.

The working principle is first introduced conceptually using a block-diagram and subsequently the governing equations and numerical implementation are described in more detail. Finally, the iterative optimization procedure is illustrated by means of a simplified test case.

The performance of the technique is assessed in terms of spatial resolution of the velocity reconstruction. A three-dimensional sine-wave lattice is used to determine the range of resolved wavenumbers. Data from a direct numerical simulation (Bernardini and Pirozzoli 2011) is used to simulate an experiment over a turbulent boundary layer.

The focus of the study lies on the comparison of the TSA reconstructions obtained with different time-segment lengths. In addition, the technique is compared to VIC+ (reconstruction based on instantaneous particle tracking velocity and its time derivative) and tomographic PIV (analysis by spatial 3D cross-correlation).

2. Time-segment assimilation (TSA)

The TSA concept is schematically illustrated in figure 1 with a block diagram. On the left, a simulation is started from an initial vorticity field (e.g. zeros) and compared to particle tracking

measurements in an iterative procedure to find the optimal initial condition (middle block). The disparity between the simulated vorticity and that estimated on the basis of the measured particles velocity yields a residual. Minimizing such residual brings the process to convergence where the vorticity and velocity fields best fit those measured along the entire time segment (right). The procedure is outlined in detail in the following sections. The section is concluded with a numerical illustration of the iterative optimization technique using a simplified test case.
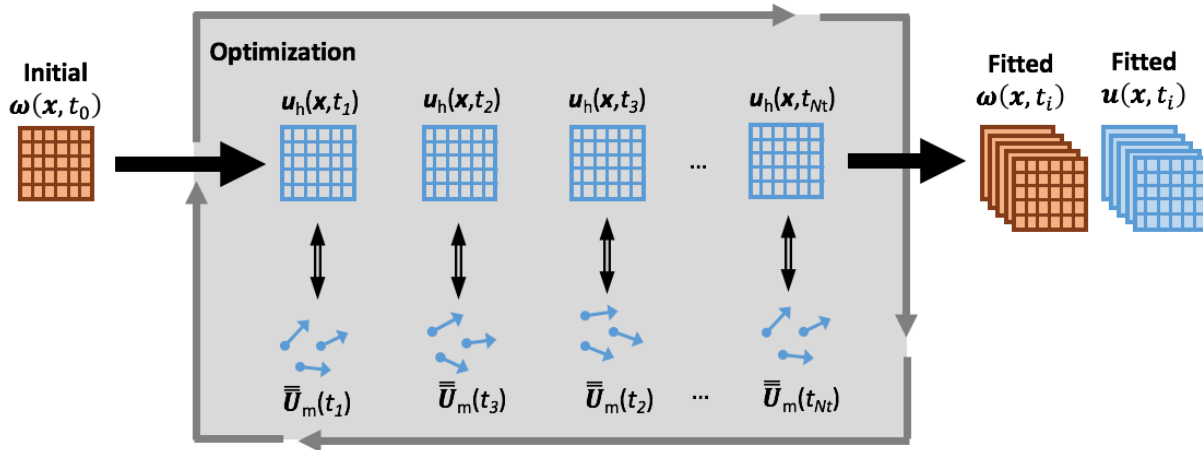
Fig. 1 Schematic illustration of iterative flow reconstruction using full particle trajectories.

2.1. Measurement data

The TSA approach is meant for applications to data obtained from volumetric particle tracking techniques such as tomographic PTV (Novara and Scarano 2013) and Shake-the-Box (Schanz et al. 2016). These methods yield velocity measurements along discrete particle trajectories γ_i. Velocity measurements are obtained by evaluating the particle velocity at the measurement time-instants t_i from for example by means of a polynomial fit. The measurement is usually represented as a set of spatially scattered velocity measurements at regularly spaced time intervals, corresponding to the timing used for image acquisition:

(1) $$\bar{\bar{U}}_m(t_i) = \{u_{\gamma_1}(x_{\gamma_1(t_i)}, t_i), u_{\gamma_2}(x_{\gamma_2(t_i)}, t_i), \dots, u_{\gamma_N}(x_{\gamma_N(t_i)}, t_i)\},$$

where N is the number of particles detected inside the measurement volume at time instant t_i. The subscript m denotes the measured particle velocity.

2.2. Optimization problem

The goal of the optimization problem is to find the temporal evolution of a velocity field $u_s(x, t)$ that extends the scattered velocity measurements $\bar{\bar{U}}_m$ to the entire measurement volume on the

measurement time-segment $[t_1, t_K]$, where $t_K = t_1 + K\Delta t$. The problem formulation is similar to that stated by Saumier et al. (2016), but instead of considering a short two-snapshot time-segment $[t_1, t_1 + \Delta t]$, here the time-segment may include a large, yet finite, number of time instants, usually with regular time-separation Δt. The velocity field distribution and temporal evolution is assumed to be consistent with the vorticity transport equation that is governing the flow temporal evolution.

Analogous to Schneiders and Scarano (2016) and Saumier et al. (2016), the incompressible and inviscid vorticity transport equation is chosen as governing equation for the flow evolution,

$$(2) \qquad \begin{cases} \frac{\partial \boldsymbol{\omega}}{\partial t} + (\boldsymbol{u} \cdot \nabla)\boldsymbol{\omega} = (\boldsymbol{\omega} \cdot \nabla)\boldsymbol{u}, \\ \boldsymbol{\omega}(\boldsymbol{x}, t_1) = \boldsymbol{\omega}_0(\boldsymbol{x}), \quad \boldsymbol{x} \in \Omega, \quad t \in [t_1, t_K], \end{cases}$$

where $\boldsymbol{\omega} = \nabla \times \boldsymbol{u}$ is the vorticity. The initial vorticity field, $\boldsymbol{\omega}_0(\boldsymbol{x})$, is numerically integrated in time using a vortex-particle discretization (vortex-in-cell, Christiansen 1973). Within the vortex-in-cell (VIC) framework, velocity is calculated from vorticity at each integration time-instant by solution of a Poisson equation,

$$(3) \qquad \nabla^2 \boldsymbol{u} = -\nabla \times \boldsymbol{\omega},$$

where it is assumed that boundary conditions are selected that make the equations well-posed. In case no boundary conditions can be defined *a-priori*, they can be considered as additional unknowns and increase the degrees of freedom in the optimization procedure. The above assumptions have been discussed in Schneiders and Scarano (2016).

Solving (2) and (3) for the time-segment $[t_1, t_K]$ yields the velocity temporal evolution in this measurement time-segment. At every measurement time-instant t_i, the gridded velocity field can be interpolated to the instantaneous particle locations to yield

$$(4) \qquad \bar{\bar{\boldsymbol{U}}}_h(t_i) = \left\{ \boldsymbol{u}_h\big(\boldsymbol{x}_{\gamma_1(t_i)}, t_i\big), \boldsymbol{u}_h\big(\boldsymbol{x}_{\gamma_2(t_i)}, t_i\big), \dots, \boldsymbol{u}_h\big(\boldsymbol{x}_{\gamma_N(t_i)}, t_i\big) \right\}.$$

This allows for calculation of the difference between the particle tracking measurements $\bar{\bar{\boldsymbol{U}}}_m$ and the result of the numerical simulation $\bar{\bar{\boldsymbol{U}}}_h$:

$$(5) \qquad J\big(\boldsymbol{\omega}_0; \bar{\bar{\boldsymbol{U}}}_m\big) = \sum_{i=1}^{K} \left| \bar{\bar{\boldsymbol{U}}}_h(t_i) - \bar{\bar{\boldsymbol{U}}}_m(t_i) \right|^2.$$

This difference, also called cost function, measures the quality of the numerical simulation, considering the measurements as a reference.

In the present work, the boundary conditions are kept fixed (i.e. based on an *a-priori* estimation) and only the initial vorticity field is taken as degree of freedom. The optimization problem is accordingly defined by:

$$(6) \qquad \arg\min_{\boldsymbol{\omega}_0} J\big(\boldsymbol{\omega}_0; \bar{\bar{\boldsymbol{U}}}_m\big).$$

The study by Saumier et al. (2016) shows that adding a term that penalizes kinetic energy in the velocity field $\boldsymbol{u}$ guarantees strong convexity for a solution to the problem considering two measurement time-instants and small Δt. The strength of the penalization, however, impacts the obtained solution. Schneiders and Scarano (2016) show that without further penalization, convergence to acceptable solutions in practical and real-world cases can be achieved. Similarly, no further penalization term to guarantee a convex minimization is included in (6) for the present study.

2.3. Numerical implementation

The vortex-in-cell framework (VIC, Christiansen 1973) is used for discretization and numerical integration of the initial condition given in terms of 3D vorticity field. In particular, the implementation by Schneiders et al. (2014) for application to volumetric PIV measurements is followed. One relevant change has been applied to the procedure to reduce its computational cost. Instead of the M4' approach (Monaghan 1985) the more classical cloud-in-cell (CIC, Christiansen 1973) technique is used for vortex particle regridding.

 The grid where vorticity and velocity are defined is a three-dimensional Cartesian grid with constant grid node spacing h. The VIC simulation yields $\boldsymbol{u}_h(\boldsymbol{x}, t)$ along the measurement time-segment $[t_1, t_K]$, which are interpolated by linear interpolation in time and space to obtain $\bar{\bar{\boldsymbol{U}}}_h$ at each measurement time-instant.

 The optimization problem is solved iteratively using the gradient-based limited memory BFGS (Liu and Nocedal 1989) algorithm. The gradient is calculated from the adjoint code (Giering and Kaminski 1998), similar to Schneiders and Scarano (2016). In the present study, the iterative procedure is started assuming that the initial vorticity field is null everywhere.

 The iterative procedure and the adjoint is illustrated below with a simplified numerical problem.

2.4. Numerical illustration

Consider a test problem where the instantaneous velocity of two tracer particles (black dots in Fig. 2) is measured (red arrows). The top row of Fig. 2 illustrates from left to right the result of the first three iterations of the iterative TSA procedure. The bottom row shows the adjoint (i.e. $\partial J/\partial\boldsymbol{\omega}$) obtained after each iteration. The initial condition for TSA (top-left in Fig. 2) is set to a vorticity field that is null everywhere. This yields also an initial velocity field that is null everywhere; hence the cost function (Fig. 3) is non-zero at the first iteration.
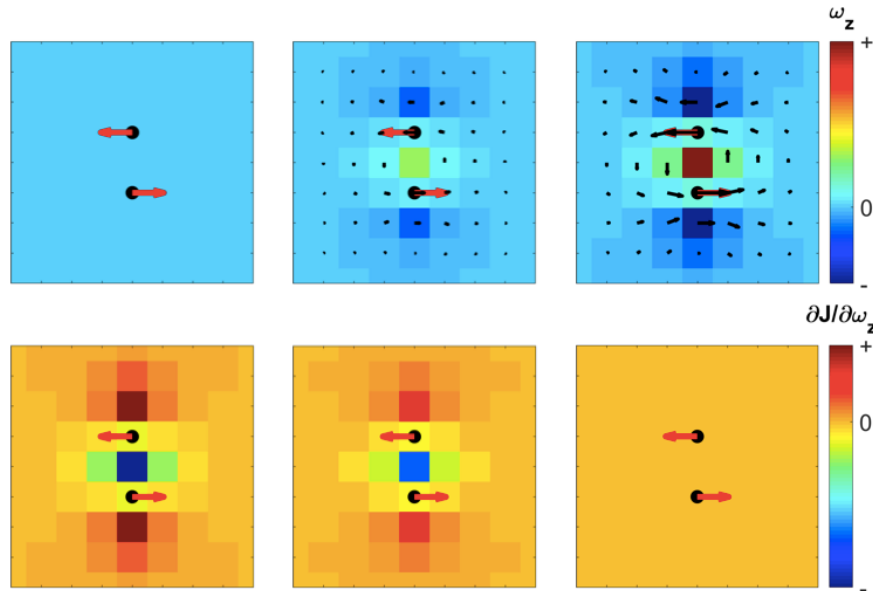
Fig. 2 Result of the first three TSA iterations (from left to right). The top row shows the initial vorticity fields and the bottom row the corresponding gradients $\partial J / \partial \boldsymbol{\omega}$ obtained from the adjoint.

The adjoint provides the gradient $\partial J / \partial \boldsymbol{\omega}$, which is plotted for the first iteration in the bottom-left figure in Fig. 2. The figure shows that when the vorticity in the center is increased, the cost function reduces (i.e. negative $\partial J / \partial \boldsymbol{\omega}_z$ in the center). Therefore, in the second iteration (middle figures), the vorticity in the center needs to be increased. This induces a velocity field similar to that of a point vortex. The cost function at the second iteration is reduced as a consequence of this updated velocity field (Fig. 3).

The distribution of the cost function gradient after the second iteration (Fig. 2-middle) remains similar to the previous iteration, inducing advancement of the solution in the same direction as for the first iteration, increasing further the vorticity in the center. This is what the optimization procedure performs, and with the third iteration (top-right figure) a stronger vortex in the domain center is obtained. The induced velocity field now almost perfectly matches the two measurement points, yielding a practically zero cost function (Fig. 3).

After the third iteration, the cost function is practically null everywhere, indicating that the optimization has converged. This is confirmed by verification that after the fourth iteration, the cost function does not change its value (Fig. 3) and the optimization procedure is stopped.
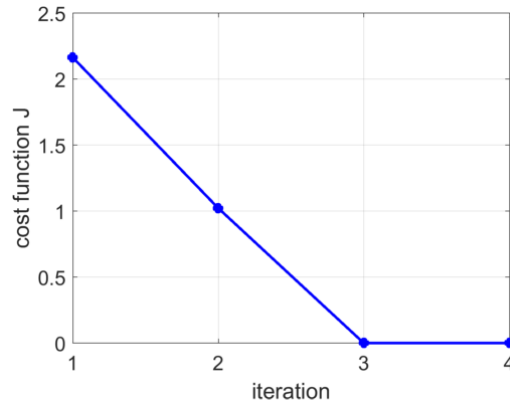
Fig. 3 Cost function values for the first four iterations.

3. Spatial resolution analysis by sinusoidal input

The use of sinusoidal velocity field as input signal to determine the amplitude modulation of the response is widely documented from early works in 2D PIV (Willert and Gharib, 1991; Scarano and Riethmuller, 2000; Scarano, 2003; Schrijer and Scarano, 2008).

The use of the normalized amplitude response test for 3D PIV measurements has been reported in Novara et al. (2012) for the analysis of spatially adaptive interrogation by cross-correlation and in the recent study of Schneiders and Scarano (2017) where the spatial resolution of VIC+ was examined.

Here a velocity field based on a sine-wave lattice is simulated with the following properties:

$$(7) \quad \begin{cases} u = A \sin\frac{2\pi x}{\Lambda} \sin\frac{2\pi y}{\Lambda} \\ v = A \cos\frac{2\pi x}{\Lambda} \cos\frac{2\pi y}{\Lambda} \\ w = A \end{cases}$$

where the wave amplitude is $A = 2$ voxels and the wavelength Λ, is varied between 20 and 500 voxels. Particles trajectories are sampled over 10 recordings. The measurements volume extends over $L_x \times L_y \times L_z = 300 \times 200 \times 200$ voxels. The tracer particle concentration is $C = 5 \times 10^{-5}$ particles per voxel (ppv). The errors arising from imperfect particle reconstruction errors are neglected in order to isolate the sole effect of spatial resolution (ideal response). The u-component of the velocity field is plotted in Fig. 4, in case of $\Lambda = 76$ voxels. The particle trajectories over a time-segment of 10 snapshots are indicated by the black lines.
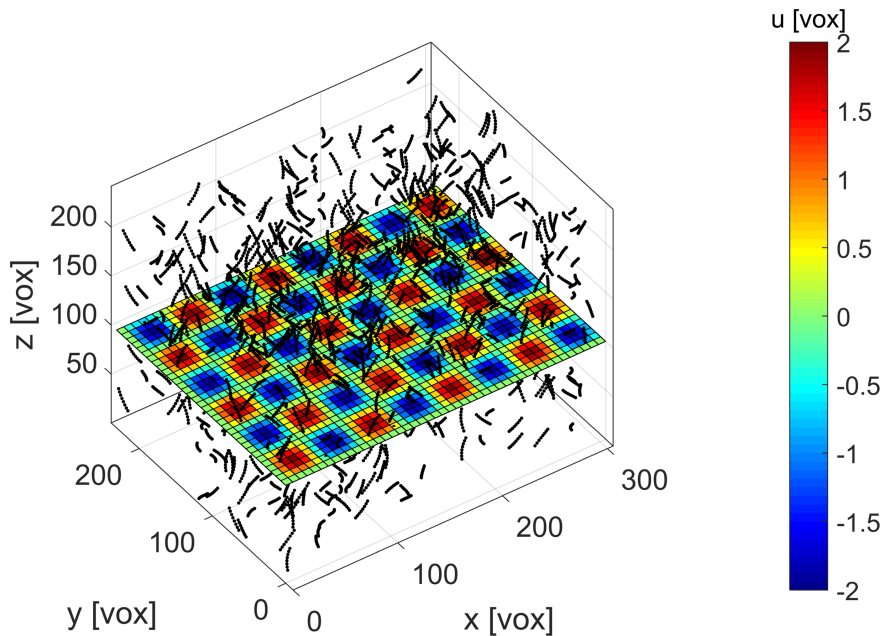
Fig. 4 Reference velocity field and particle tracking measurements ($K = 10$) in the case of $\Lambda = 76$ voxels.

The grid spacing for the proposed technique is set equal to that adopted for VIC+ data post-processing (Schneiders and Scarano 2016) and is based on the criterion $h = 0.25C^{-1/3}$. This yields a vector spacing of 7 voxels. For practical reasons concerning the computational cost, the iterative procedure is limited to 50 iterations for all cases.

The thumbnail in Figure 5 illustrates the results of the sine waves analysis. The particles concentration is kept constant through the analysis. The first row shows the effect of changing the sinusoid wavelength maintaining the number of exposures fixed to a minimum of 2. The ratio of particle distance to wavelength $l^* = < r >/ L$ is varied from 0.1 (left) to 0.8 (right). The results of the first row are comparable to what is obtained with the VIC+ analysis where the instantaneous particles velocity and acceleration are used for the problem optimization. The lattice of sinusoids is accurately described for the largest wavelength. The reconstruction remains acceptable at intermediate level ($l^* = 0.4$). At the smallest value of wavelength, the analysis fails to return the correct number and their location.
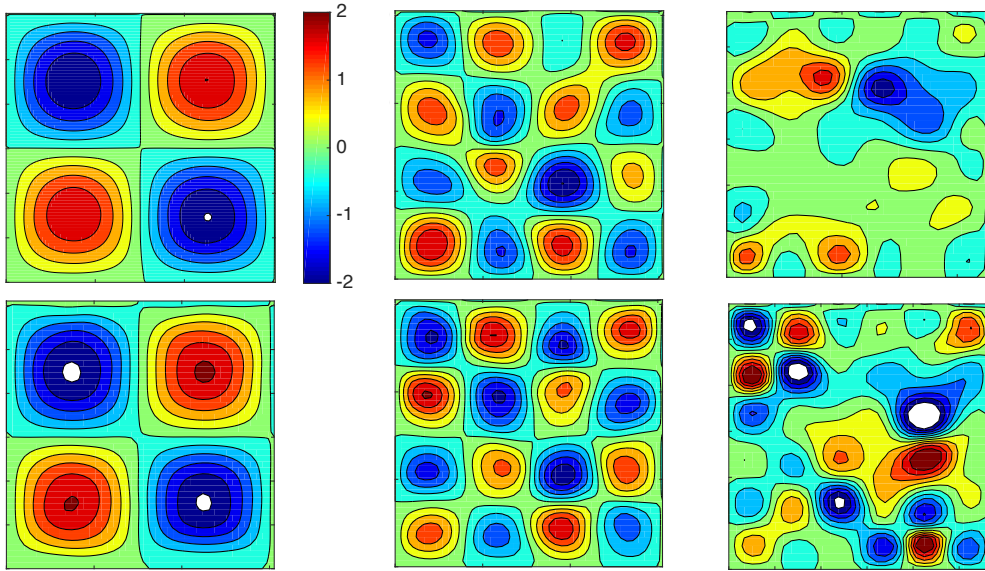
Fig. 5 Reconstructed u-component of velocity with 2 (top row) and 50 exposures (bottom row).

In the second row the same analysis has been obtained varying the number of recordings from a minimum of 2 up to a maximum of 51.

The difference to the upper case is minimal for the longest wavelength ($l^* = 0.1$). At the intermediate value, the reconstruction of the sinusoids pattern returns higher peaks, indicating a smaller effect of spatial modulation. The position of the peaks is also improved.

At the smallest wavelength, the reconstruction retrieves approximately 50% of the local peaks.Similar shortcomings as the case with fewer exposures are observed, with the reconstruction occasionally failing to retrieve local peaks and their position.

3.1. Normalised amplitude response

A more synthetic view of the above is given in Figure 6 that shows the amplitude modulation u/u_0 obtained by the different velocity reconstruction techniques considered. On the horizontal axis, the normalized wavenumber is given by $l^* = IV/\Lambda$, where IV is the interrogation volume size used for the 3D cross-correlation analysis (each interrogation volume contains on average 5 particles). The amplitude modulation is defined as the ratio of peak streamwise velocity in the measurement volume in comparison to the reference provided by Eq. (7). The tomographic PIV (green line) and VIC+ results (blue line) are taken from Schneiders et al. (2017). The squared sinc function is plotted for comparison, as literature reports a flatter spatial response of iterative cross-correlation with window deformation compared to a squared sinc function (Schrijer and Scarano 2008). The red lines indicate the results using the proposed full-track reconstruction technique with a 2-snapshots kernel (dashed lines) and a 10-snapshots kernel (solid line).
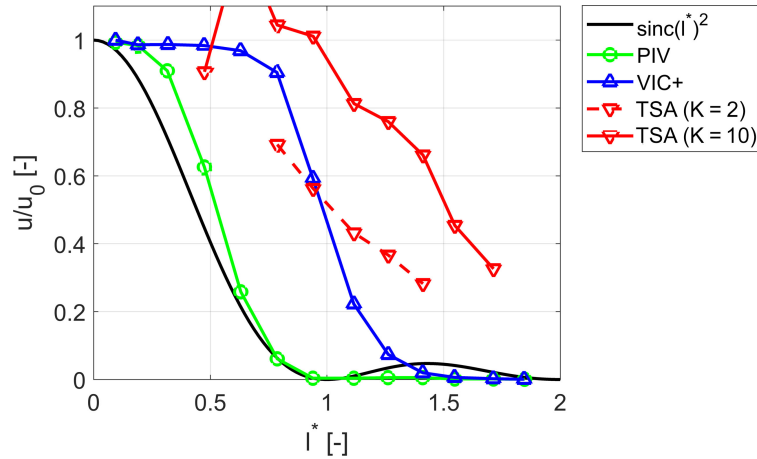
Fig. 6 Amplitude modulation of a range of velocity measurement techniques. The red lines indicate the results using the proposed full-track reconstruction technique with a 2-snapshot kernel (dashed lines) and a 10-snapshot kernel (solid line).

The results are encouraging and concerning at the same time. Figure 6 indicates that increasing the length of the time-segment considered for the optimization from $k = 2$ snapshots to $k = 10$ snapshots potentially increases the cut-off l^* defined at $u/u_0 = 0.5$ from approximately $l^* = 1$ to $l^* = 1.5$. This corresponds to a reduction of the smallest resolvable scale by approximately 30%. The latter translates in a requirement of seeding concentration lowered by approximately a factor four.

However, in a specific range of normalized wavenumbers ($0.5 < l^* < 1$) the peak of velocity the fluctuations appears to be overestimated, concerning the analysis with 10 snapshots time segment. Further studies need to address this behavior examining factors such as grid resolution, stability and convergence of the algorithm.

4. Turbulent boundary layer

Particle tracking measurements are considered in a turbulent boundary layer ($u_\infty = 10$ m/s, $\delta_{99} = 9.4$ mm), simulated from a direct numerical simulation (DNS) by Bernardini and Pirozzoli (2011). The same dataset was used previously for assessment of the VIC+ technique by Schneiders and Scarano (2016). The Reynolds number based on boundary layer thickness is $Re_\delta = 8185$. This numerical simulation was used previously for assessment of tomographic PIV processing techniques by Pröbsting et al. (2013) and Lynch and Scarano (2015). The salient boundary layer parameters are summarized in Table 1.

The simulated tracer particle concentration is 50 particles/δ_{99}^3, corresponding to the lowest seeding concentration case in Schneiders et al (2016).

Tab. 1 Boundary layer parameters for the numerical assessment

Free stream velocity	u_∞	10 m/s
Boundary layer thickness	δ	9.4 mm
Momentum thickness	θ/δ	0.12
Shape factor	H	1.50
Reynolds number	Re_δ (Re_θ)	8185 (1000)

Figure 7-left shows the result using 2 consecutive particle tracking velocity measurements, visualized vortices identified by the Q-Criterion (red) and iso-surfaces of low-speed streaks (green). The right figure shows the result from the optimization using a data ensemble of 10 consecutive velocity measurements. The black arrow indicates the distance over which the flow is convected (based on the free-stream velocity) over the considered time-segments.
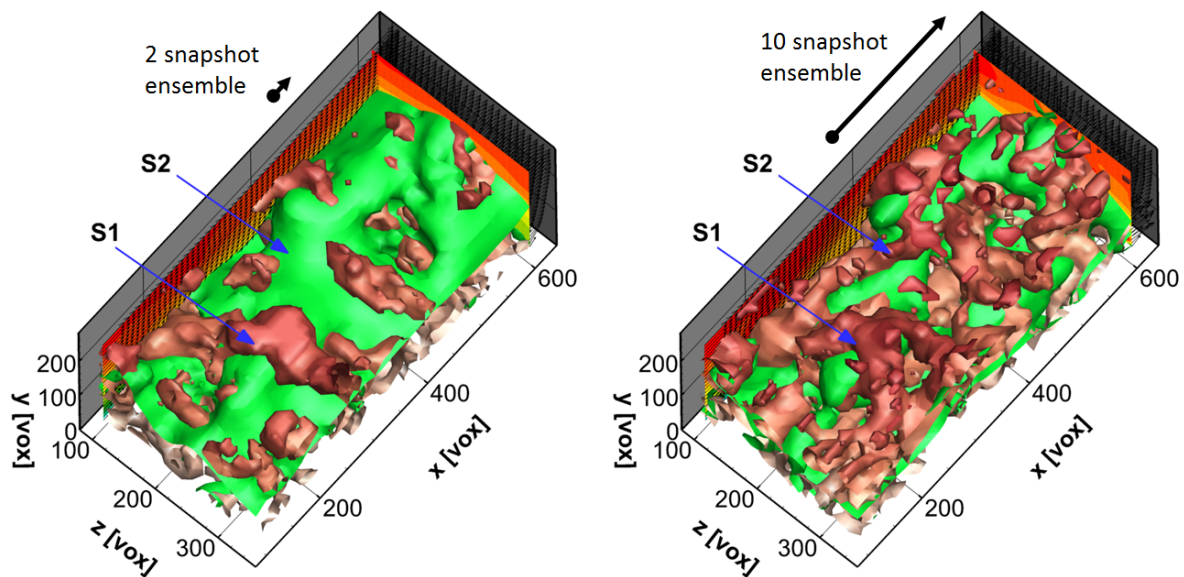
Fig. 7 Simulated turbulent boundary layer measurement visualized by isosurfaces of Q-criterion (red) and $u'/u_\infty = -0.05$ (green). Reconstruction using 2 (left) and 10 (right) consecutive velocity measurements. The distance over which the flow is convected with free-stream velocity over the data domain is indicated by the black arrows.

The inspection of the results using a short (left) and long (right) time-segment suggests that the latter yields a richer flow field in terms of vortical structures. Whereas the relatively large structure S1 is reconstructed using a 2-snapshot ensemble, the smaller structure S2 is only recovered with an extended number of 10 consecutive velocity measurements.

The above confirms qualitatively the main findings in the previous section that flow structures with a smaller wavelength can be recovered by using an extended number of snapshots for instantaneous flow reconstruction using the vorticity transport equation. The application to real data is an ongoing effort, where attention is placed on the effect of measurement noise as a possible source of error amplification.

5. References

Bernardini M, Pirozzoli S (2011) Wall pressure fluctuations beneath supersonic turbulent boundary layers. Phys Fluids 23:085102.

Christiansen JP (1973) Numerical simulation of hydrodynamics by the method of point vortices. J Comput Phys 13:363–379.

de Silva CM, Philip J, Marusic I (2013) Minimization of divergence error in volumetric velocity measurements and implications for turbulence statistics. Exp Fluids 54:1557.

Gesemann S, Huhn F, Schanz D, Schröder A (2016) From noisy particle tracks to velocity, acceleration and pressure fields using B-splines and penalties. In: 18th Int. Symp. on Applications of Laser and Imaging Techniques to Fluid Mechanics. Lisbon, Portugal. 4–7 July.

Giering R, Kaminski T (1998) Recipes for adjoint code construction. ACM Trans Math Softw 24(4):437–473.

Liu DC, Nocedal J (1989) On the limited memory method for large scale optimization. Math Program B 45:503–528.

Monaghan JJ (1985) Extrapolating B splines for interpolation. J Comput Phys 60:253–262.

Novara M, Scarano F (2013) A particle-tracking approach for accurate material derivative measurements with tomographic PIV. Exp Fluids 54:1584.

Novara M, Ianiro A, Scarano F (2012) Adaptive interrogation for 3D-PIV. Meas. Sci. Technol. 24:024012.

Saumier L-P, Khouider B, Agueh M (2016) Effective filtering and interpolation of 2D discrete velocity fields with Navier–Stokes equations. Inverse Problems. 32:115006.

Scarano F, Riethmuller ML (2000) Advances in iterative multigrid PIV image processing. Exp Fluids 29(Supplement 1):S051–S060.

Scarano F, (2003) Theory of non-isotropic spatial resolution in PIV. Exp Fluids 35:268–277.

Schanz D, Gesemann S, Schröder A (2016) Shake the box: Lagrangian particle tracking at high particle image densities. Exp. Fluids 57:70. doi:10.1007/s00348-016-2157-1.

Schiavazzi D, Coletti F, Iaccarino G, Eaton JK (2014) A matching pursuit approach to solenoidal filtering of three-dimensional velocity measurements. J. Comput. Phys. 263:206-221.

Schneiders JFG, Azijli I, Scarano F, Dwight RP (2015) Pouring time into space. 11th International Symposium on Particle Image Velocimetry, Santa Barbara, CA, September 14-16.

Schneiders JFG, Scarano F (2016) Dense velocity reconstruction from tomographic ptv with material derivatives. Exp Fluids 57:139.

Schneiders JFG. Scarano F, Elsinga GE (2017) Resolving vorticity and dissipation in a turbulent boundary layer by tomographic PTV and VIC+. Exp. Fluids. 58:27.

Schrijer FFJ, Scarano F (2008) Effect of predictor–corrector filtering on the stability and spatial resolution of iterative PIV interrogation. Exp Fluids 45:927–941.

Willert CE, Gharib M (1991) Digital particle image velocimetry. Exp. Fluids 10:181-193.